

RESEARCH ARTICLE

10.1002/2017JD028016

Key Points:

- Western Tibetan Plateau summer snow anomalies affect East Asian climate
- Processes of western and southern Tibetan Plateau snow over influences are different
- Snow anomalies over western Tibetan Plateau are linked to a wave train pattern from the North Atlantic

Correspondence to:

R. Wu,
renguang@mail.iap.ac.cn

Citation:

Wang, Z., Wu, R., Chen, S., Huang, G., Liu, G., & Zhu, L. (2018). Influence of western Tibetan Plateau summer snow cover on East Asian summer rainfall. *Journal of Geophysical Research: Atmospheres*, 123, 2371–2386. <https://doi.org/10.1002/2017JD028016>

Received 7 NOV 2017

Accepted 11 FEB 2018

Accepted article online 20 FEB 2018

Published online 1 MAR 2018

Influence of Western Tibetan Plateau Summer Snow Cover on East Asian Summer Rainfall

Zhibiao Wang^{1,2}, Renguang Wu^{1,3} , Shangfeng Chen¹ , Gang Huang³ , Ge Liu⁴ , and Lihua Zhu^{2,3,5}

¹Center for Monsoon System Research, Institute of Atmospheric Physics, Chinese Academy of Sciences, Beijing, China, ²School of Earth Science, University of Chinese Academy of Sciences, Beijing, China, ³State Key Laboratory of Numerical Modeling for Atmospheric Sciences and Geophysical Fluid Dynamics, Institute of Atmospheric Physics, Chinese Academy of Sciences, Beijing, China, ⁴Chinese Academy of Meteorological Sciences, China Meteorological Administration, Beijing, China, ⁵School of Atmospheric Sciences/Plateau Atmosphere and Environment Key Laboratory of Sichuan Province/Joint Laboratory of Climate and Environment Change, Chengdu University of Information Technology, Chengdu, China

Abstract The influence of boreal winter-spring eastern Tibetan Plateau snow anomalies on the East Asian summer rainfall variability has been the focus of previous studies. The present study documents the impacts of boreal summer western and southern Tibetan Plateau snow cover anomalies on summer rainfall over East Asia. Analysis shows that more snow cover in the western and southern Tibetan Plateau induces anomalous cooling in the overlying atmospheric column. The induced atmospheric circulation changes are different corresponding to more snow cover in the western and southern Tibetan Plateau. The atmospheric circulation changes accompanying the western Plateau snow cover anomalies are more obvious over the midlatitude Asia, whereas those corresponding to the southern Plateau snow cover anomalies are more prominent over the tropics. As such, the western and southern Tibetan Plateau snow cover anomalies influence the East Asian summer circulation and precipitation through different pathways. Nevertheless, the East Asian summer circulation and precipitation anomalies induced by the western and southern Plateau snow cover anomalies tend to display similar distribution so that they are more pronounced when the western and southern Plateau snow cover anomalies work in coherence. Analysis indicates that the summer snow cover anomalies over the Tibetan Plateau may be related to late spring snow anomalies due to the persistence. The late spring snow anomalies are related to an obvious wave train originating from the western North Atlantic that may be partly associated with sea surface temperature anomalies in the North Atlantic Ocean.

1. Introduction

Snow is an important component in the climate system. Snow variability affects surface energy budget and the hydrology cycle (Barnett et al., 1989; Cohen & Rind, 1991; Yasunari et al., 1991). The Tibetan Plateau has a large snow cover area in the cold seasons (Pu et al., 2007; Z. Wang et al., 2017). Numerous studies have demonstrated impacts of the cold season Tibetan Plateau snow change on Indian and East Asian climate (e.g., Chen & Wu, 2000; Dey & Kumar, 1983; Ding et al., 2009; Fasullo, 2004; Hahn & Shukla, 1976; Kripalani et al., 2003; Ose, 1996; Si & Ding, 2013; C. Wang et al., 2017; Wu & Kirtman, 2007; Wu et al., 2010; Xiao & Duan, 2016; Zhang et al., 2004; Zhao et al., 2007; Zuo et al., 2012; Zhu et al., 2015). However, due to the lack of station observations at the high-elevation region (You et al., 2008) and the small snow cover area in summer (Z. Wang et al., 2017), few studies have been conducted on the summer snow variations over the Tibetan Plateau and their impacts on the climate variability.

Recently, several studies have investigated the effects of summer snow cover over the Tibetan Plateau on regional climate using satellite retrieved snow data (Liu, Wu, & Zhang, 2014; Wu et al., 2012, 2016). Wu et al. (2012) showed that the Tibetan Plateau snow cover modulated the effect of El Niño-Southern Oscillation on the East Asian summer monsoon. They indicated that the El Niño-Southern Oscillation signals tend to be stronger in summers with reduced Tibetan Plateau snow cover. Liu, Wu, and Zhang (2014) revealed an effect of the summer Tibetan Plateau snow cover change on precipitation in the Mei-Yu-Baiu region. Wu et al. (2016) identified a linkage of the summer heat wave frequency in the southern Europe and northeastern Asia regions with anomalous summer snow cover over the Tibetan Plateau. The snow cover influence on local energy budget is likely more crucial in summer due to the high solar elevation angle. However, the local relationship between the summer snow cover and surface heat flux variations over the

Plateau are not yet clear. Such relationship provides a basis for understanding whether the snow changes are a response to or a driving factor of atmospheric anomalies. In the present study, one issue to be addressed is the local relationship between the interannual variations of summer snow cover and surface variables over the Tibetan Plateau.

Liu, Wu, and Zhang (2014) considered the Tibetan Plateau snow anomaly as a whole in their investigation of the effect of summer snow cover on circulation and precipitation over East Asia. They indicated that the impacts of summer Tibetan Plateau snow cover change on circulation and precipitation over East Asia are realized through modulating the North India Ocean convection, a tropical overturning west-east circulation, the tropical western North Pacific convection, and then a meridional circulation pattern along the East Asian coast. They noted that the midlatitude Asian circulation changes were not involved in the link between the summer Tibetan Plateau snow cover and East Asian rainfall variations. Our analysis shows that interannual variations of summer snow cover are different in western and southern Plateau regions. As such, the whole Tibetan Plateau snow cover as a single index may not be able to capture properly the influence of the regional snow cover anomalies. Thus, a second issue to be addressed in the present study is the different impacts and the associated processes of summer snow cover anomalies in different regions of the Tibetan Plateau on circulation and precipitation over East Asia.

Snow anomalies in a specific season may also related to the snow mass in the preceding season due to the persistence of snow anomalies (Liu, Wu, Zhang, & Nan, 2014; Z. Wang et al., 2017; Wu & Kirtman, 2007; Wu et al., 2014). For example, Liu, Wu, Zhang, and Nan (2014) showed that the summer snow anomalies over the Tibetan Plateau may already exist in preceding May, which provides a precursory signal for summer rainfall anomalies. A question is what the source of summer snow cover anomalies over the Tibetan Plateau is. Thus, a third issue to be addressed in the present study is the plausible factors and related processes of interannual variations of summer snow cover over the western Tibetan Plateau.

In the following, section 2 presents the data sets and methods used in this study. We document the mean and interannual variation of summer snow cover and the local snow-surface heat flux relationship over the Tibetan Plateau in section 3. In section 4, we address circulation and precipitation changes associated with the western and southern Tibetan Plateau snow cover anomalies and the associated connecting processes. Section 5 discusses the source of the Tibetan Plateau snow cover anomalies. Summary and discussions are provided in section 6.

2. Data and Methods

The snow cover and snow water equivalent used in the present study were obtained from the National Snow and Ice Data Center (<http://nsidc.org/data/>). The Northern Hemisphere snow cover of version 4.1 was generated from the advanced very high resolution radiometer, the Geostationary Operational Environmental Satellite System, and other visible-band satellite data (Brodzik & Armstrong, 2013). The original weekly snow cover data cover the period from October 1966 to December 2016 with a 25 km spatial resolution. The weekly snow cover data were converted to monthly mean with regular $1^\circ \times 1^\circ$ longitude-latitude grids for the present analysis (Z. Wang et al., 2017). The global snow water equivalent data were derived from Scanning Multichannel Microwave Radiometer (1978–1987), and selected Special Sensor Microwave or Imagers (1987–2007) (Armstrong et al., 2005) with a 25 km spatial resolution, and also were converted to regular $1^\circ \times 1^\circ$ longitude-latitude grids.

Monthly mean variables of horizontal winds at 10 m, soil temperature and soil moisture at 0–10 cm, surface latent heat net flux, sensible heat net flux, downward solar radiation flux, upward solar radiation flux, downward longwave radiation flux, upward longwave radiation flux, and precipitation rate used in this study are from the National Centers for Environmental Prediction (NCEP)–Department of Energy (DOE) reanalysis 2 (Kanamitsu et al., 2002). The reanalysis data are provided by the National Oceanic and Atmospheric Administration/Office of Oceanic and Atmospheric Research/Earth System Research Laboratory (NOAA/OAR/ESRL) Physical Science Department (PSD) (<https://www.esrl.noaa.gov/psd/>). The surface reanalysis variables are on T62 Gaussian grids and available from January 1979 to the present.

Monthly mean geopotential height, winds, and vertical wind velocity at pressure levels with a spatial resolution of $1.25^\circ \times 1.25^\circ$ were obtained from the Japanese 55-year Reanalysis (JRA-55) (Kobayashi et al., 2015).

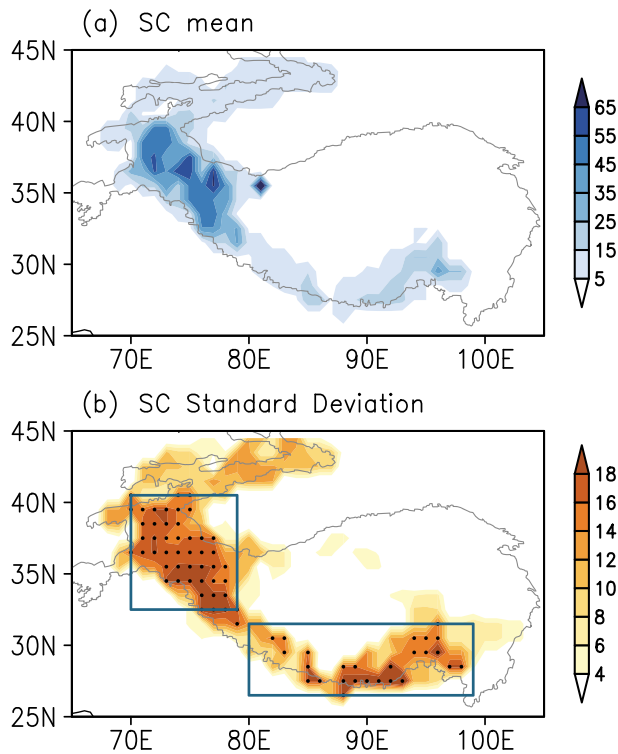


Figure 1. Distribution of (a) mean (%) and (b) interannual standard deviation (%) of JJA snow cover for the period 1979–2015 based on the National Snow and Ice Data Center data. The two box covered areas in (b) denote the domains of the west region and the south region. The curves denote the 3,000 m elevation (same in other figures). The dotted regions at (b) denote standard deviation significant at the 95% confidence level.

The JRA-55 reanalysis data are provided by Climate Prediction Division, Global Environment and Marine Department at Japan Meteorological Agency (<http://jra.kishou.go.jp/JRA-55/>). The JRA-55 reanalysis data are available from January 1958 to present.

The monthly precipitation data used in the present study is the Global Precipitation Climatology Project (GPCP) version 2.3 (Adler et al., 2003). The GPCP precipitation data are provided by NOAA/OAR/ESRL PSD (<https://www.esrl.noaa.gov/psd/>) with a $2.5^\circ \times 2.5^\circ$ spatial resolution and are available from January 1979 to present.

The monthly surface air temperature and cloud were acquired from the University of East Anglia Climate Research Unit (CRU) of version ts4.00 (<http://www.cru.uea.ac.uk/data/>) (Harris et al., 2014). The CRU data are on the $0.5^\circ \times 0.5^\circ$ spatial resolution and span the period from 1901 to 2016.

The monthly mean sea surface temperature (SST) was from the Centennial In Situ Observation-Based Estimates of the Variability of Sea Surface Temperature (COBE-SST) provided by Tokyo Climate Center, Climate Prediction Division at Japan Meteorological Agency (Ishii et al., 2005). The COBE-SST data were obtained from NOAA/OAR/ESRL PSD (<https://www.esrl.noaa.gov/psd/>) with a spatial resolution of $1^\circ \times 1^\circ$ and covering the period from January 1891 to present.

The present study focuses on the interannual variability in summer. So the monthly data were filtered by a 9 year low-pass Gaussian filter to extract the interannual variability. A linear regression analysis is applied to investigate the statistical relationships between year-to-year variations of the Tibetan Plateau snow cover and other variables. A composite analysis is used to document regional circulation and precipitation changes at different snow cover situations over the

Tibetan Plateau. The significance level of correlation coefficient and regressed and composite anomalies is estimated based on the Student's *t* test. In the present study, summer refers to June–July–August (JJA).

3. Local Effects of Summer Tibetan Plateau Snow Cover Changes

In this section, we first compare the JJA snow cover variations in the western and southern Tibetan Plateau. Then, we illustrate the ability of two snow cover indices, which are constructed based on area-mean snow cover anomalies in the western and southern Plateau, to represent interannual variations of regional snow cover. At last, we analyze related anomalies in surface air temperature, soil temperature and soil moisture of 0–10 cm layer, surface heat fluxes, and total atmospheric column heat source to unravel the local effects of snow cover anomalies.

The JJA mean snow cover over the Tibetan Plateau is confined to the western and southern part (Figure 1a). In comparison, the mean snow cover is larger in the western part than in the southern part (Figure 1a). The standard deviation displays a distribution similar to the mean value with large values over the western part and along the southern hill region (Figure 1b). Note that the interannual variability of snow cover in the southern region is comparable to that in the western region although the mean value is smaller in the southern region.

According to the distribution of JJA snow cover mean and standard deviation, we select two regions to construct area-mean snow cover changes. The two regions are marked using the boxes in Figure 1b, which are denoted as, respectively, the west region ($70^\circ\text{E}–79^\circ\text{E}$, $32.5^\circ\text{N}–40.5^\circ\text{N}$) and the south region ($80^\circ\text{E}–99^\circ\text{E}$, $26.5^\circ\text{N}–31.5^\circ\text{N}$). The area-mean snow cover is calculated by averaging the values of snow cover anomalies at the grids within the respective box. The obtained area-mean JJA snow cover anomalies are shown in Figure 2. The area-mean JJA snow cover in the west region displays large year-to-year fluctuations during 1990s, whereas the variability is small before late 1980s and displays a reduction after late 1990s (Figure 2a). The area-mean JJA snow cover in the south region displays a relatively large fluctuation in the 1980s and

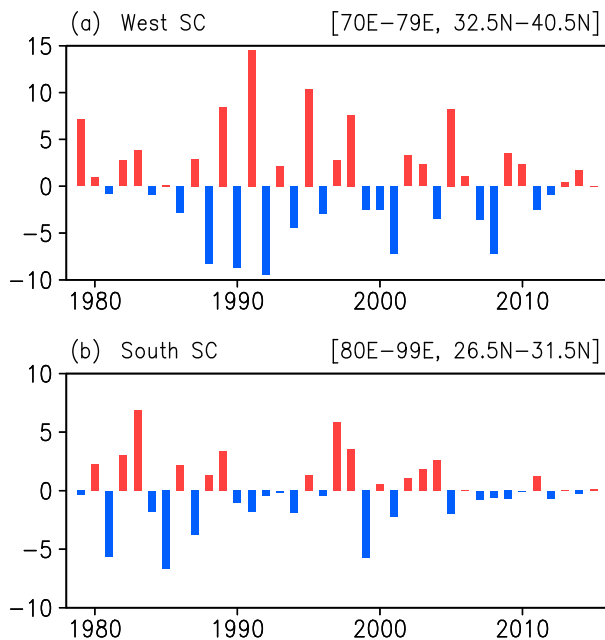


Figure 2. Time series of area-mean interannual snow cover anomalies (%) in the (a) west region and (b) south region for the period 1979–2015.

around 2000 (Figure 2b). After the middle 2000s, the interannual variations of JJA snow cover are very small in the south region (Figure 2b), which may be related to the declining trend of JJA snow cover there (Z. Wang et al., 2017). The correlation coefficient between the two time series is about 0.19 for the period 1979–2015, which is below the 90% confidence level. The above results indicate that the interannual variations of snow cover in the western and southern Plateau display different features, and thus, the whole Plateau time series may not represent the regional disparity of snow cover variations.

To validate the representativeness of two regional mean snow cover anomalies for grid snow cover variations in the two regions, we regress the grid snow cover and snow water equivalent anomalies against the time series of area-mean snow cover anomalies over the western and southern Plateau region. The snow cover and snow water equivalent anomalies corresponding to the time series of the west region snow cover are confined to the western Plateau (Figures 3a and 3b). The snow cover anomalies corresponding to the time series of the south region snow cover are large in the southern part and extend to the southern portion of the western Plateau (Figure 3c), but the snow water equivalent anomalies are relatively small in the southern Plateau and large in the southwestern Plateau region (Figure 3d). The westward shift in the location of snow water equivalent anomalies relative to snow cover anomalies may be related to the

dependence on the distribution of mean snow mass that is larger in a western portion of the southern Plateau (Z. Wang et al., 2017). The above distribution indicates that it is proper to use the area-mean snow cover time series to represent the JJA snow cover variations in the two regions.

We examine anomalies of surface heat fluxes, surface air temperature, and soil temperature at 0–10 cm by regression on the snow cover indices to investigate the local effect of the snow cover anomalies on the atmosphere. Corresponding to more snow cover in the western Plateau, there is an increase in upward shortwave

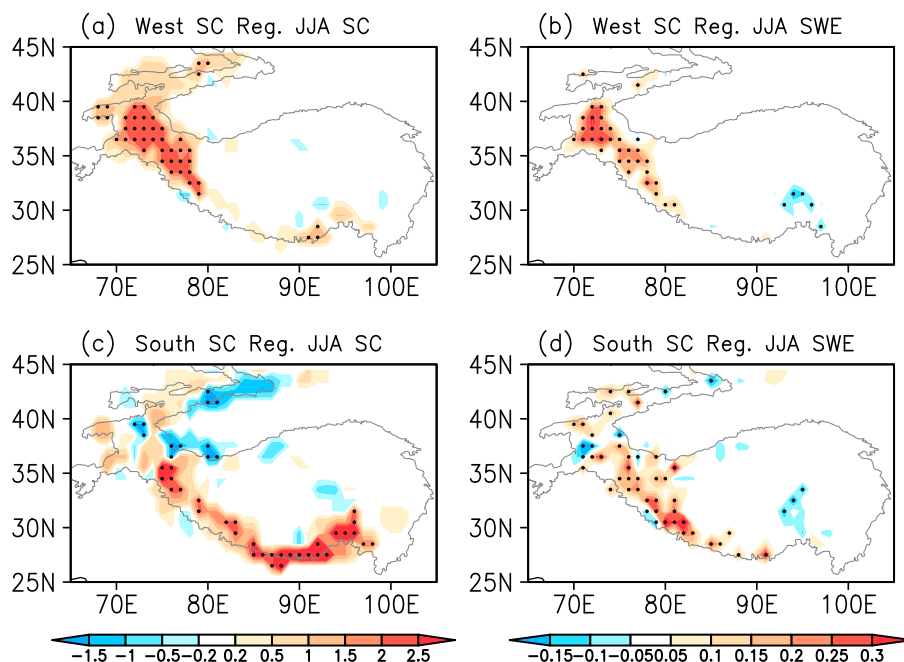


Figure 3. Anomalies of June–July–August (JJA) (left) snow cover (%) and (right) snow water equivalent (mm) obtained by linear regression against JJA interannual snow cover index in (a and b) the west region and (c and d) the south region. The dotted regions denote anomalies significant at the 95% confidence level.

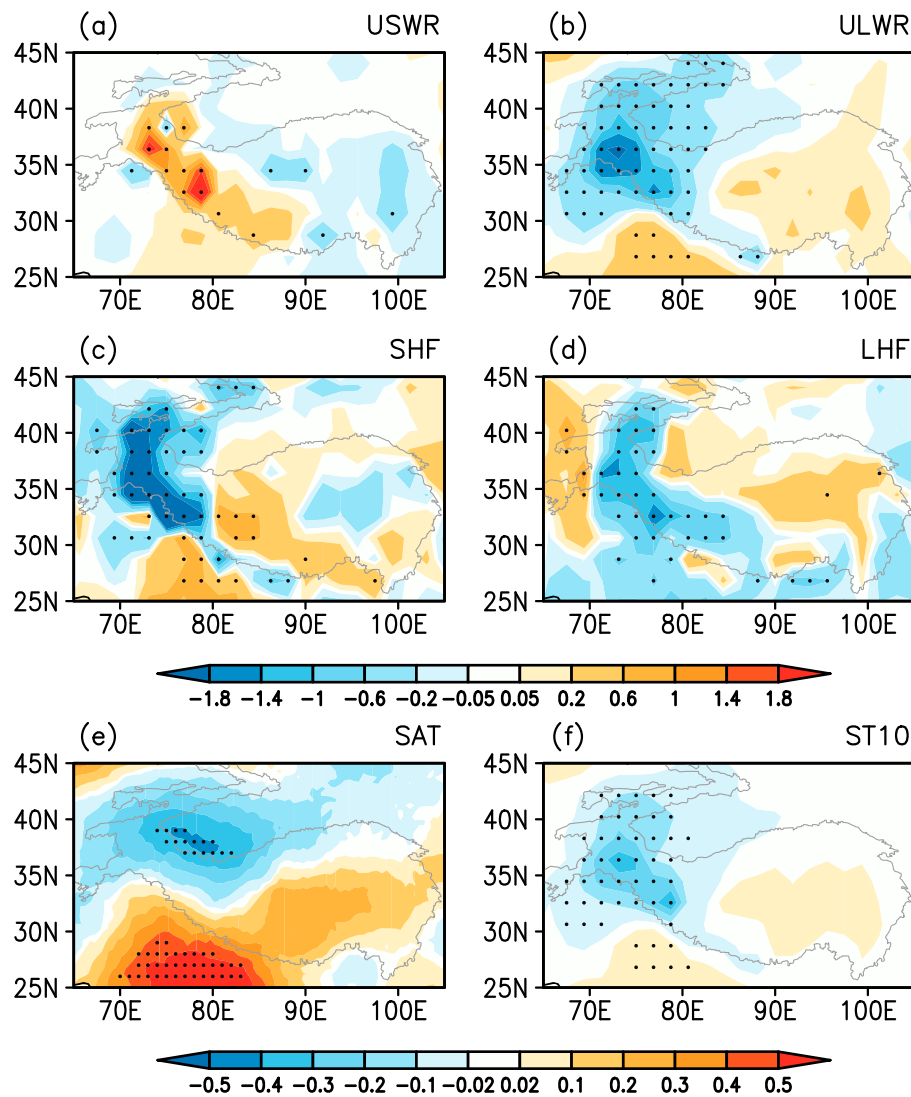


Figure 4. Anomalies of June–July–August (a) upward shortwave radiation (w/m^2), (b) upward longwave radiation (w/m^2), (c) sensible heat flux (w/m^2), (d) latent heat flux (w/m^2), (e) surface air temperature ($^{\circ}C$), and (f) soil temperature at 0–10 cm ($^{\circ}C$) obtained by linear regression against June–July–August interannual snow cover index in the west region. The dotted regions denote anomalies significant at the 95% confidence level.

radiation there (Figure 4a), which signifies the albedo effect of snow cover. This results in a decrease in shortwave radiation absorbed by the surface, leading to a decrease in land surface temperature. This is confirmed by negative soil temperature anomalies in the western Plateau (Figure 4f). Following the surface temperature decrease, upward longwave radiation from the land surface is reduced (Figure 4b). As the presence of snow intercepts the energy exchange between the land surface and the overlying atmosphere, more snow cover reduces upward sensible and latent heat fluxes (Figures 4c and 4d), resulting the decline in surface air temperature (Figure 4e). Here we note that the reanalysis latent heat flux used in the present study is calculated based on the bulk formula and the snow sublimation effect may not be considered properly. As more snow is expected to increase snow sublimation, the sublimation-related latent heat flux anomalies may be opposite to the reanalysis-based latent heat flux anomalies. This may cancel part of negative latent heat flux anomalies obtained in the present analysis. The largest surface air temperature decrease is located in the northern part (Figure 4e). The difference in the location between the snow cover and surface air temperature decrease regions may be due to the contribution of atmospheric processes to surface air temperature variations. The cloud decrease is more obvious in southern portion of the snow decrease region so that the downward shortwave radiation reaching the Earth’s surface increases more in southern portion (figures not shown).

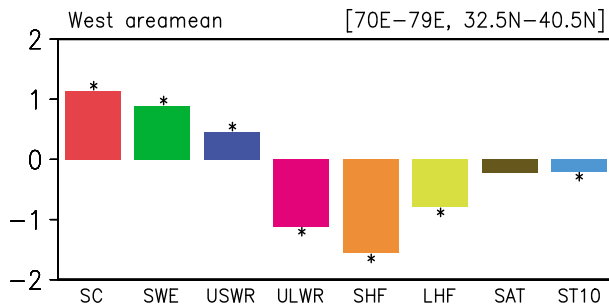


Figure 5. Anomalies of June-July-August snow cover (SC) (%), snow water equivalent (SWE) (0.1 mm), upward shortwave radiation (USWR) (w/m^2), upward longwave radiation (ULWR) (w/m^2), sensible heat flux (SHF) (w/m^2), latent heat flux (LHF) (w/m^2), surface air temperature (SAT) ($^{\circ}\text{C}$), and soil temperature at 0–10 cm (ST10) ($^{\circ}\text{C}$) averaged over the west region obtained by linear regression against June-July-August interannual snow cover index in the west region. The asterisk denotes anomalies significant at the 95% confidence level.

The surface anomalies associated with the western Plateau snow cover changes are further examined using area-mean values in the west region. More snow cover and snow water equivalent are accompanied by an increase in reflected upward shortwave radiation, a decrease in sensible and latent heat fluxes, a decrease in upward longwave radiation, and a decrease in land and surface air temperature (Figure 5). These changes signify the effects of snow by altering the surface albedo and suppressing the energy exchange between the land surface and the overlying atmosphere. Similar anomalies are observed in association with the southern Plateau snow cover changes but with a smaller magnitude (figure not shown) likely because the southern hill region cannot be well resolved in the reanalysis. Overall, the results indicate an impact of the Plateau summer snow cover anomalies on the atmosphere.

To confirm the effect of snow anomalies on the atmosphere, we have calculated total heat source in the atmospheric column (Q1) following the method of Zhao and Chen (2001). Climatologically, the central and eastern Tibetan Plateau is a large heat source in summer (Figure 6a), consistent with previous studies (e.g., Yanai et al., 1992; Zhao & Chen, 2001). The western Plateau is a heat sink region in summer, which agrees with the presence of snow cover (Figure 1a). The Q1 anomalies unravel clearly the effects of snow anomalies. Corresponding to more snow cover over the western Plateau, atmospheric cooling covers the western and southwestern parts and atmospheric heating is present in the eastern region (Figure 6b). The largest cooling is observed in the southwestern part likely due to the dependence on the mean state. Climatologically, large mean precipitation is observed along the southern hills of the Tibetan Plateau where there is large topography-related mean wind convergence. As the precipitation variability tends to be larger in regions where there is more mean precipitation, precipitation-related atmospheric heating and cooling tend to be larger in this region. Accordingly, the atmospheric cooling anomalies are larger over the southern and southwestern parts (Figure 6c).

4. Remote Impacts of Summer Tibetan Plateau Snow Cover Changes

Previous section showed that the summer snow cover anomalies over the Tibetan Plateau may induce anomalous heating in the overlying atmosphere. As such, the snow effects may be induced in remote regions. In this section, we document the circulation and precipitation changes in the surrounding regions associated with the summer snow cover anomalies over the Tibetan Plateau.

Corresponding to more snow cover over the western Plateau, an obvious wave pattern is observed over the midlatitude Asia at the upper level (Figure 7a). The wave pattern consists of an anomalous cyclone over the western Tibetan Plateau, an anomalous anticyclone over the eastern Tibetan Plateau, and an anomalous cyclone over Northeast China. Such a wave train is a dominant mode of upper-level wind variations during boreal summer over the midlatitude Asia (Lu et al., 2002; Wu, 2002). At lower level, an anomalous cyclone is observed over Northeast China (Figure 7b). To the south of the cyclone are anomalous southwesterly winds that transport more moist air from lower latitudes, which is accompanied by above-normal rainfall extending from the Yangtze River to east of Japan (Figures 7a and 7b). Above-normal rainfall is observed over the equatorial central Pacific, which is overlaid by lower-level anomalous westerlies and upper-level anomalous easterlies. Below-normal rainfall over tropical western North Pacific is associated with an anomalous lower-level anticyclone. Below-normal rainfall is also observed over North India where lower-level anomalous winds display divergence. Liu, Wu, and Zhang (2014) noted that the midlatitude Asian circulation pattern is not involved in the influence of the summer Tibetan Plateau snow cover anomalies on the East Asian rainfall. Here we show an obvious wave pattern over the midlatitude Asia. The discrepancy may be attributed to the difference in the region used to obtain the summer Tibetan Plateau snow cover anomalies. There are several regions where the rainfall variations have a significant correlation with the summer snow cover anomalies over the western Tibetan Plateau. To quantify the relationship, we calculate the correlation coefficient of area-mean rainfall in the four regions as denoted by the boxes in Figure 7b with the western Plateau snow cover. The obtained correlation coefficient is -0.48 (reaching the 99% confidence level), $+0.49$ (reaching

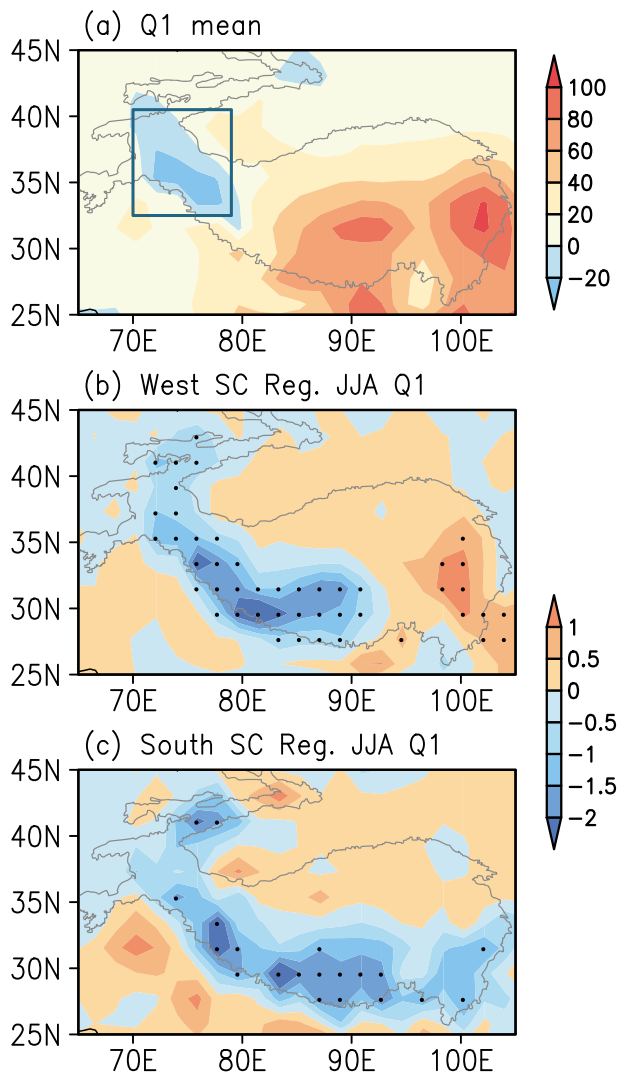


Figure 6. Distribution of (a) June–July–August (JJA) mean Q1 (w/m^2) and JJA Q1 anomalies (w/m^2) obtained by linear regression against JJA interannual snow cover index in (b) the west region and (c) the south region. The covered areas in (a) denote the domain of the west region. The dotted regions in (b) and (c) denote anomalies significant at the 95% confidence level.

the 99% confidence level), -0.36 (reaching the 95% confidence level), and $+0.30$, respectively, in the four regions for the period 1979–2015 (Table 1).

Corresponding to more snow cover over the southern Tibetan Plateau, large anomalous westerlies are observed over tropical Indian Ocean at the upper level (Figure 7c). Over the midlatitude, an elongated anomalous cyclone extends from the Tibetan Plateau to the North Pacific. At lower level, an anomalous cyclone covers East Asia (Figure 7d). Over the equatorial central Pacific are anomalous easterlies at upper level and anomalous westerlies at lower level (Figures 7c and 7d). Above-normal rainfall is observed in the region extending from the Yangtze River to east of Japan (Figures 7c and 7d), consistent with lower-level anomalous westerlies. There is more rainfall in the equatorial central Pacific. Rainfall experiences a decrease over the tropical western North Pacific in association with upper-level convergence and lower-level divergence of anomalous winds. Above-normal rainfall is observed in the Arabian Sea where there is convergence of anomalous lower-level winds. The distribution of wind and rainfall anomalies is quite similar to that obtained by Liu, Wu, and Zhang (2014) based on the whole Plateau snow cover. In particular, we note opposite wind anomalies at the lower level and upper level over the North Indian Ocean and the South China Sea and a west-east contrast of rainfall anomalies between the Arabian Sea and tropical western North Pacific. This forms an anomalous east-west overturning circulation as Liu, Wu, and Zhang (2014). Along the East Asian coast, a meridional wave pattern is observed at lower level, accompanied by alternative negative-positive-negative rainfall anomalies. This feature is also similar to that of Liu, Wu, and Zhang (2014). These results appear to confirm Liu, Wu, and Zhang (2014) for the processes of impact of the summer Tibetan Plateau snow cover anomalies on the East Asian summer rainfall. To quantify the relationship, we calculate the correlation coefficient of area-mean rainfall in the four regions as denoted by the boxes in Figure 7d with the southern Plateau snow cover. The obtained correlation coefficient is $+0.35$ (reaching the 95% confidence level), $+0.41$ (reaching the 95% confidence level), -0.54 (reaching the 99% confidence level), and $+0.34$ (reaching the 95% confidence level), respectively, in the four regions for the period 1979–2015 (Table 1).

Comparing the wind and rainfall anomalies corresponding to the western and southern Plateau snow cover changes, there are both differences and common features. Notable differences are mainly observed in the Indian Ocean sector. The wind anomalies are more significant over the tropical

Indian Ocean corresponding to the southern Plateau snow cover, but over the midlatitude Asia corresponding to the western Plateau snow cover. Large rainfall anomalies appear in the North Indian Ocean corresponding to the southern Plateau snow cover, but in North India corresponding to the western Plateau snow. The wind and rainfall anomalies tend to display similar features in the western Pacific sector. In comparison, the magnitude of precipitation anomalies over East Asia and tropical western Pacific induced by southern Plateau snow cover anomalies is larger than that induced by western Plateau snow cover anomalies. The above comparison indicates that both the western and southern Plateau snow cover anomalies may influence the East Asian circulation and rainfall. However, the difference in the Indian Ocean sector suggests that the physical processes for the influence are different. The southern Plateau snow cover anomalies appear to follow the paths proposed by Liu, Wu, and Zhang (2014). The influence of the western Plateau snow cover anomalies is through the midlatitude Asian wave pattern.

In view of the difference of snow cover variations between the western and southern Plateau regions, it is meaningful to examine the anomalies with respect to the difference of western and southern Plateau snow cover anomalies. For this purpose, we construct a new snow cover index using the difference of western

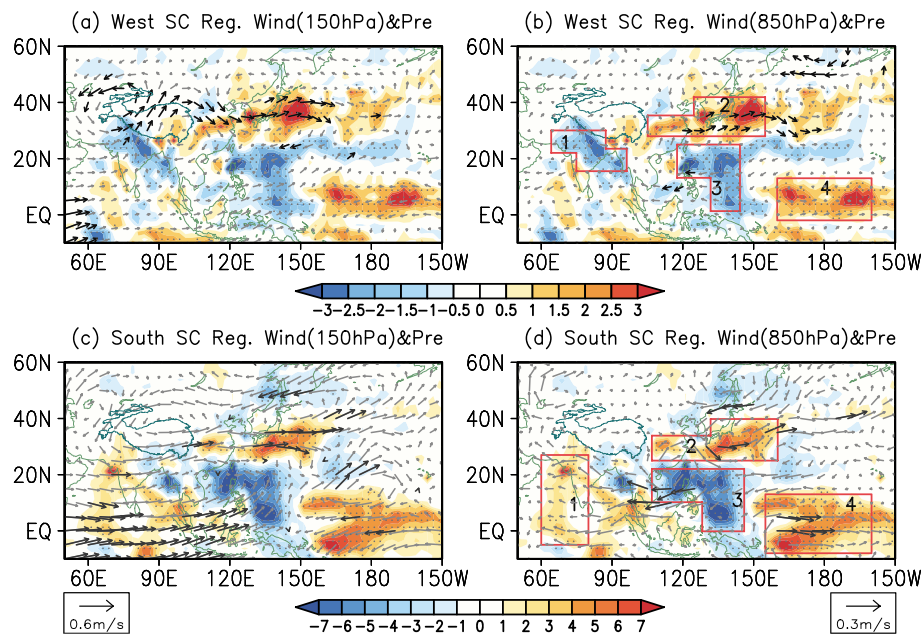


Figure 7. Anomalies of June–July–August (left column) winds (m/s) at 150 hPa and precipitation (mm/month) and (right column) winds (m/s) at 850 hPa and precipitation (mm/month) (right) obtained by linear regression against June–July–August interannual snow cover index in (a and b) the west region and (c and d) the south region. The dotted regions denote precipitation anomalies significant at the 95% confidence level, and the black vectors denote wind anomalies significant at the 90% confidence level. The red box covered areas in (b and d) denote the four domains used to calculate precipitation anomalies corresponding to the snow cover in the west region and the south region, respectively. The scale for wind vectors is shown at bottom-left (a and c) and bottom-right (b and d) corner.

minus southern Plateau JJA snow cover anomalies and then regress JJA wind and precipitation anomalies against the new snow cover index. Corresponding to positive value of the index, below-normal precipitation is observed over North India and there are anomalous upper-level cyclonic and anticyclonic winds, respectively, to the west of the Tibetan Plateau and over eastern Tibetan Plateau (Figure 8a). These features are similar to those corresponding to more snow cover over western Plateau (Figure 7a). Over East Asia, the above-normal rain band and associated upper-level anomalous winds shift northward compared to those corresponding to western and southern Plateau snow cover anomalies (Figure 8a versus Figures 7a and 7c). The lower-level wind anomalies are not significant in most regions (Figure 8b).

Corresponding to both the western and southern Plateau snow cover anomalies, notable rainfall anomalies are observed over the equatorial central Pacific (Figure 7). This raises the question whether the equatorial Pacific warming may induce tropical Pacific heating and cooling anomalies, which then contribute to the East Asian summer rainfall changes through atmospheric teleconnection pattern over the western North Pacific and East Asia. In other words, the regressed rainfall anomalies over East Asia in Figure 7 may include impacts of the equatorial Pacific SST anomalies. Indeed, the regressed SST anomalies are positive in the equatorial eastern Pacific (Figure 9). To examine whether the Tibetan Plateau snow cover anomalies may induce

rainfall changes over East Asia without the equatorial Pacific SST influence, we remove the Niño-3 (5°S–5°N, 120°W–90°W) SST signal from the wind and rainfall anomalies using regression with respect to Niño-3 SST anomalies and redo the regression analysis. The obtained anomalies display similar features though there are some changes in the magnitude of wind and rainfall anomalies (Figures 10a and 10b). For example, the midlatitude Asian wave pattern at upper level remains corresponding to the western Plateau snow cover anomalies (Figure 10a). Large upper-level westerly anomalies are still present over the tropical Indian Ocean (Figure 10b). An anomalous lower-level cyclone and accompanying above-normal rainfall are present over East Asia (figures not shown). This indicates that the Tibetan Plateau snow cover anomalies may induce wind and rainfall changes over East Asia independent of the equatorial Pacific SST influence.

Table 1
Correlation Coefficients Between the Normalized June–July–August Interannual Snow Cover Index in the West Region and the South Region and Regional Precipitation Anomalies

West regions	1	2	3	4
SC&Pre	−0.48**	0.49**	−0.36*	0.30
South regions	1	2	3	4
SC&Pre	0.35*	0.41*	−0.54**	0.34*

Note. Refer to Figures 7b–7d for the domain of calculating the regional precipitation anomalies.

*Anomalies significant at the 95% confidence level. **Anomalies significant at the 99% confidence level.

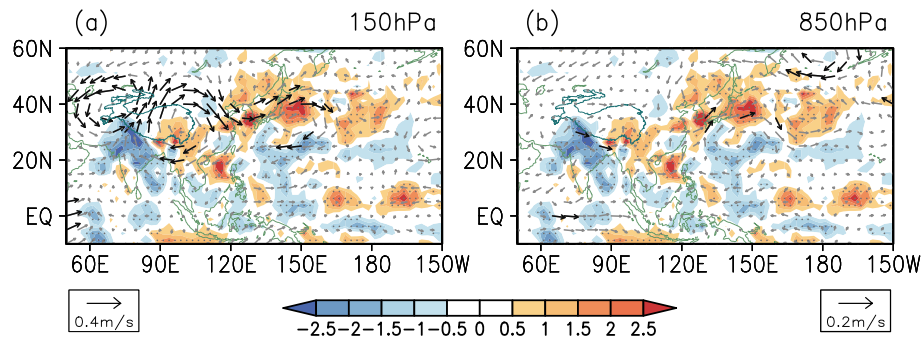


Figure 8. Anomalies of June-July-August (a) winds (m/s) at 150 hPa and precipitation (mm/month) and (b) winds (m/s) at 850 hPa and precipitation (mm/month) obtained by linear regression against the difference of June-July-August snow cover anomalies in the west region and the south region. The dotted regions denote precipitation anomalies significant at the 95% confidence level, and the black vectors denote wind anomalies significant at the 90% confidence level. The scale for wind vectors is shown at bottom-left (a) and bottom-right (b) corner.

Although the correlation coefficients between the western and southern Tibetan Plateau snow cover variations are insignificant, the similar distributions of wind and rainfall anomalies over East Asia corresponding to the western and southern Plateau snow cover anomalies indicate a combined effect. To examine the individual impacts, we redo the regression analysis after removing their interdependence. Apparently, the main features of wind and rainfall anomalies over East Asia remain corresponding to the western and southern Plateau snow cover anomalies (Figures 10c and 10d). This is consistent with the weak correlation between the western and southern Plateau snow cover variations.

To further examine the individual and combined impacts of the western Plateau snow cover anomalies, we perform a composite analysis of wind and rainfall anomalies in different combinations of western and

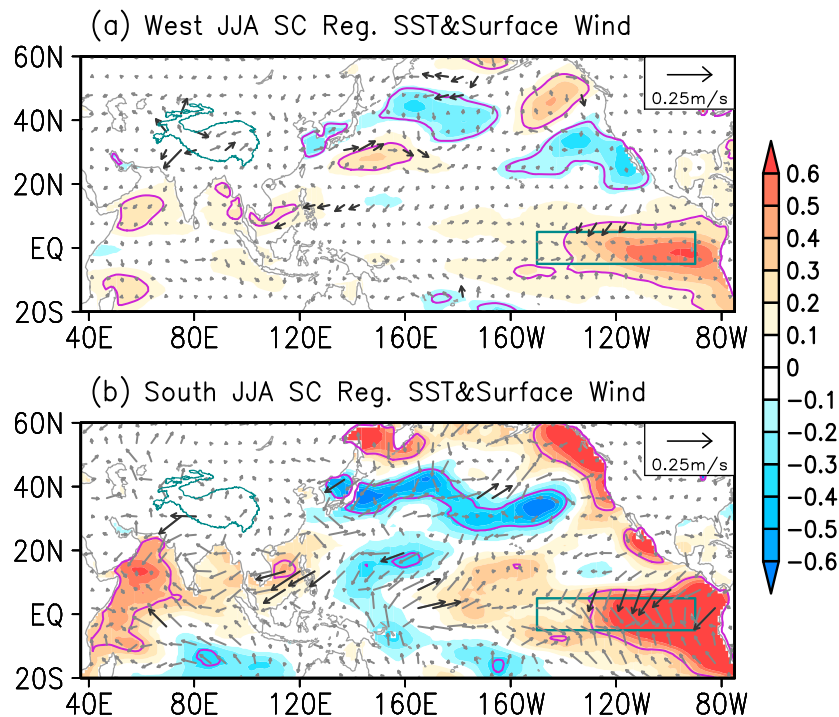


Figure 9. Anomalies of June-July-August winds at 10 m (m/s) and sea surface temperature (SST) (0.1 °C) obtained by linear regression against June-July-August inter-annual snow cover index in (a) the west region and (b) the south region. The purple contours and the black vectors denote precipitation and wind anomalies significant at the 90% confidence level. The boxed area denotes the Niño-3 region. The scale for wind vectors is shown at the top-right corner.

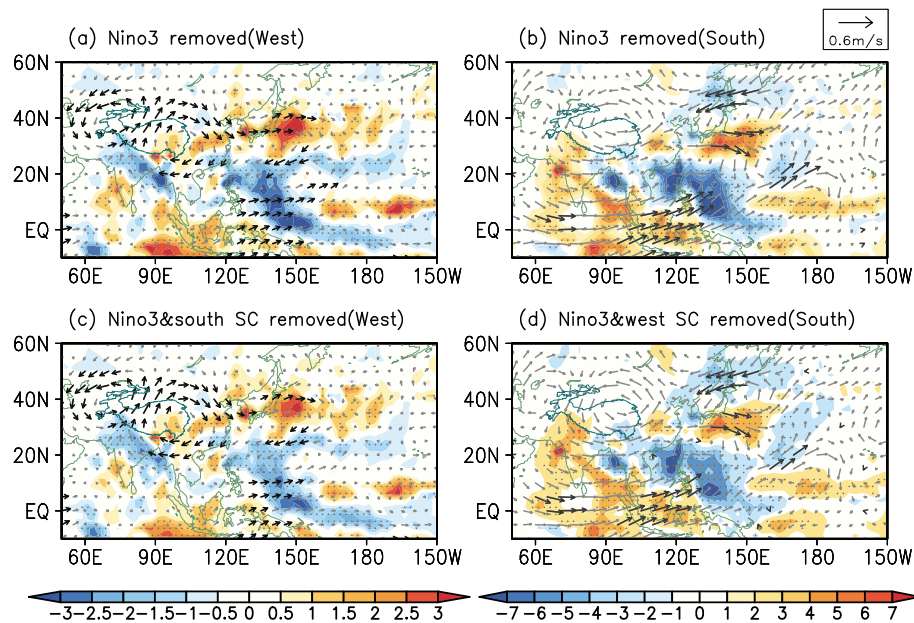


Figure 10. Anomalies of June–July–August winds (m/s) at 150 hPa and precipitation (mm/month) obtained by linear regression against June–July–August interannual snow cover index in (a) the west region and (b) the south region after removing the Niño-3 SST signal. (c and d) Similar to (a) and (b) but after removing the interdependence of snow cover anomalies in the south and west regions. The scale for wind vector is shown at top-right corner. The dotted regions denote precipitation anomalies, respectively, significant at the 95% confidence level, and the black vectors denote wind anomalies significant at the 90% confidence level.

southern Plateau snow cover anomalies. We classify a year as a positive, negative, or normal year when the western and southern Plateau snow cover index is greater than 0.4 standard deviation, less than -0.4 standard deviation, or falls in between, respectively. The 0.4 standard deviation as a criterion in the classification of years is somewhat subjective. So there are nine combinations of the western and southern Plateau snow cover anomalies. Our composite analysis is done for three types of combinations, which have relatively more samples. These are positive in the west region and normal in the south region (denoted as Positive&Normal years for brevity), negative in the west region and normal in the south region (denoted as Negative&Normal years for brevity), and positive in the west region and positive in the south region (denoted Positive&Positive years for brevity). There are 5, 6, and 7 years, respectively, in the three types of combinations (Table 2). The anomalies in the first and second types of combinations may be attributed to the western Plateau snow cover anomalies only, whereas the anomalies in the third type of combination include impacts of both western and southern Plateau snow cover anomalies.

In the Positive&Normal years, an obvious wave pattern exists over the midlatitude Asia and extends to the North Pacific at upper level (Figure 11a). At lower level, there is an anomalous cyclone over Northeast China (Figure 11b). Above-normal rainfall extends from eastern China to Japan (Figures 11a and 11b). The distribution of wind anomalies resembles that of the regressed anomalies with respect to the western Plateau snow cover anomalies. In comparison, the rainfall anomalies over East Asia appear weaker. In the Negative&Normal years, a wave pattern with nearly opposite wind anomalies appears over the midlatitude Asia (Figure 11c). Negative rainfall anomalies extend from east coast of China to east of Japan (Figures 11c and 11d), accompanied by an anomalous lower-level anticyclone though weak (Figure 11d). The wind anomalies over East Asia appear weaker, whereas those over the equatorial Pacific appear stronger compared to the Positive&Normal years. In the Positive&Positive years, the midlatitude Asian wave pattern is still present at upper level, but a zonal component appears to be included (Figure 11e). The rainfall anomalies over eastern China through Japan and over the tropical western North Pacific appear more prominent compared to the Positive&Normal years (Figure 11f). Apparently, the wind anomalies over the tropical Indian Ocean are larger and more significant (Figures 11e and 11f). Thus, the wind and rainfall features appear to be a combination of signals of the western and southern Plateau snow cover anomalies.

Negative rainfall anomalies are observed in North India corresponding to more snow cover over the western Plateau (Figure 7a). The associated cooling over North India may contribute to the midlatitude Asian wave

Table 2
The Three Combinations of Years With Different Anomalies of Normalized June-July-August Interannual Snow Cover in the West and South Regions

Types	Years
Positive&Normal	1979, 1993, 2002, 2009, 2010
Negative&Normal	1990, 1992, 1996, 2000, 2007, 2008
Positive&Positive	1982, 1983, 1989, 1995, 1997, 1998, 2003

pattern (e.g., Wu, 2002). The correlation coefficient of rainfall between the region 1 and region 2 is -0.40 (reaching the 95% confidence level). To remove the effect of the North Indian cooling, we performed a partial correlation analysis. After removing the North Indian rainfall signal, the correlation coefficient between the western Plateau snow cover and the region 2 rainfall is $+0.38$, which is significant at the 95% confidence level. Notable positive rainfall and SST anomalies are observed corresponding to more snow cover over the southern

Plateau (Figures 7d and 9b). This suggests a contribution of tropical Indian Ocean SST anomalies to the East Asian-western Pacific circulation and rainfall anomalies (Liu, Wu, & Zhang, 2014). Liu, Wu, and Zhang (2014) analyzed cases of summer Plateau snow anomalies with weak SST anomalies in the North Indian Ocean and demonstrated the role of the Plateau snow cover anomalies. We performed a partial correlation analysis regarding this issue. After removing the North Indian rainfall signal, the correlation coefficient between the southern Plateau snow cover the region 2 rainfall is 0.34 , which is significant at the 95% confidence level.

To verify the impacts of the Tibetan Plateau snow cover anomalies, we conduct model experiments with a barotropic model (Sardeshmukh & Hoskins, 1988). The barotropic model is spectral with the truncation at

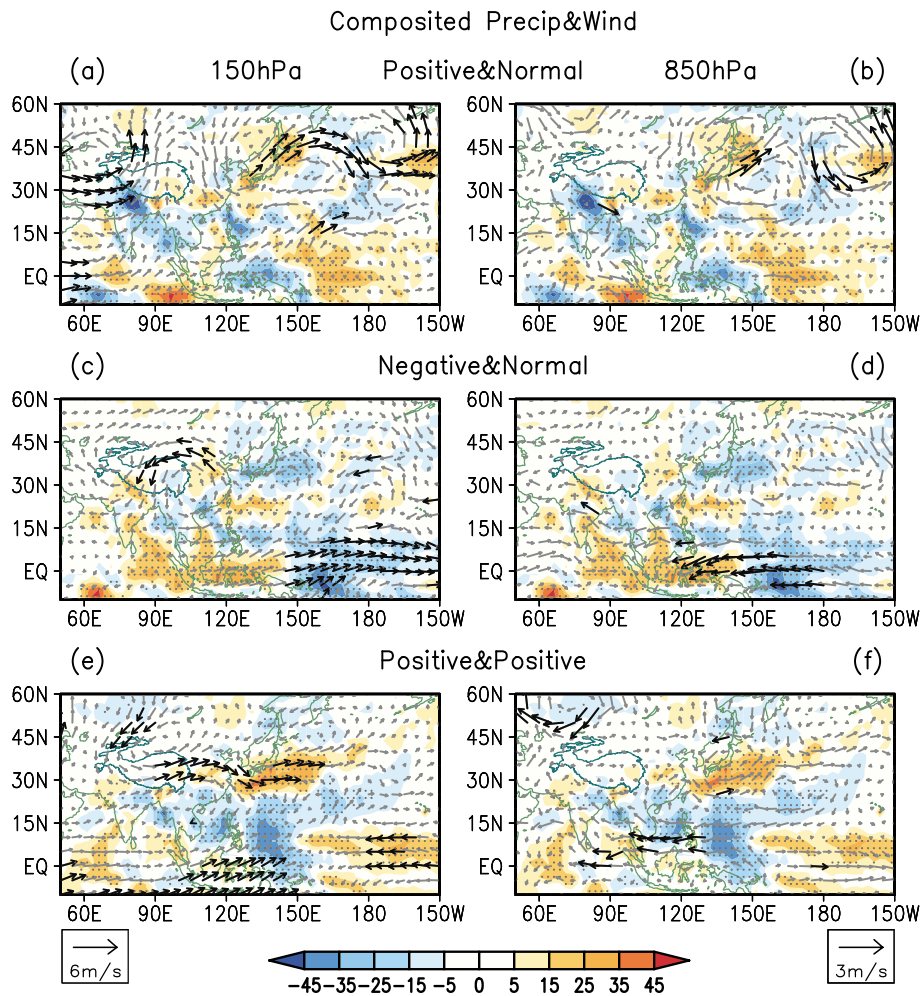


Figure 11. Composite anomalies of June-July-August (left column) winds (m/s) at 150 hPa and precipitation (mm/month) and (right column) winds (m/s) at 850 hPa and precipitation (mm/month) in the types of years with (a and b) Positive&Normal, (c and d) Negative&Normal, and (e and f) Positive&Positive snow cover anomalies in the west and south region. The dotted regions denote precipitation anomalies significant at the 95% confidence level, and the black vectors denote wind anomalies significant at the 90% confidence level. The scale for wind vectors is shown at bottom-left (a, c, and e) and bottom-right (b, d, and f) corner.

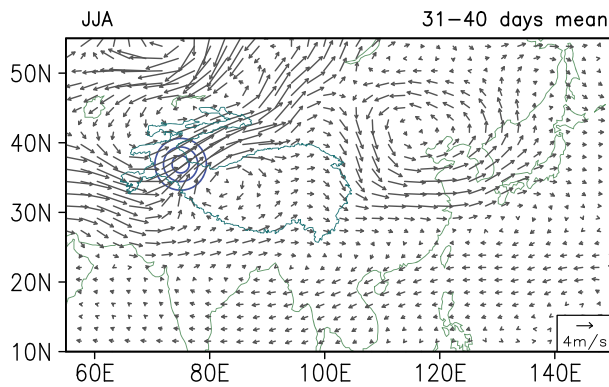


Figure 12. Barotropic model wind perturbation difference (m/s) averaged over days 31–40 and imposed idealized convergence and divergence anomaly difference (blue contours) for climatological mean winds in June–July–August (JJA). The scale for winds is shown at bottom-right corner.

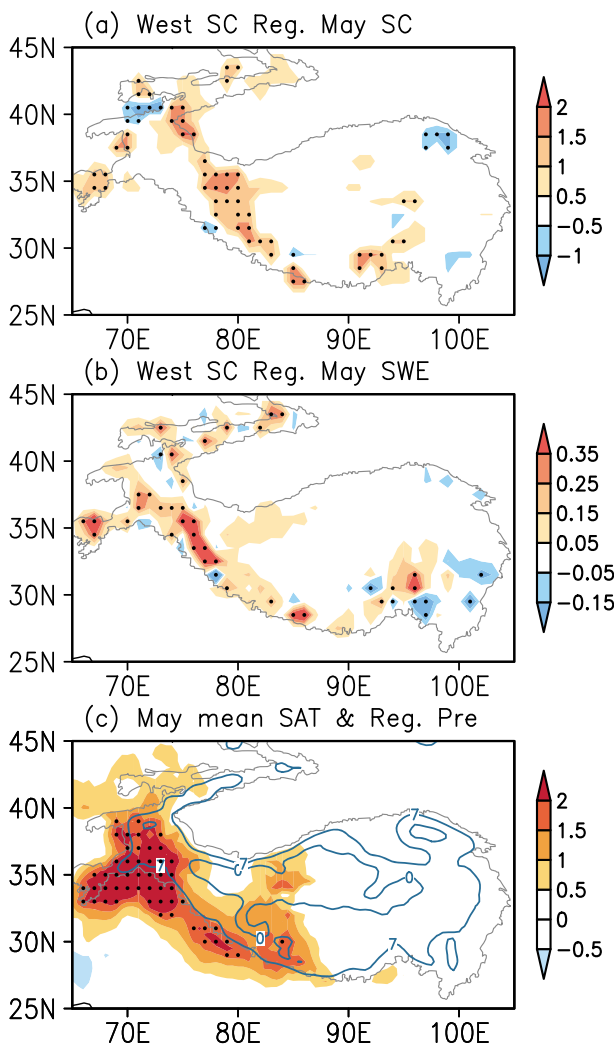


Figure 13. Anomalies of May (a) snow cover (%), (b) snow water equivalent (mm), and (c) precipitation (mm/month) obtained by linear regression against June–July–August (JJA) interannual snow cover index in the west region. The blue curves at (c) denote climatological mean temperature at 0 °C and 7 °C in May.

rhomboidal wavenumber 40. Two experiments have been conducted. In Experiment 1, climatological JJA mean divergence plus a negative convergence anomaly is specified over the western Plateau. In Experiment 2, climatological JJA mean divergence plus a positive convergence anomaly is specified in the same region. The prescribed convergence anomaly has a maximum intensity of $7 \times 10^{-6} \text{ s}^{-1}$ and centered at 37°N and 75°E (Figure 12). The location of the divergence anomaly is chosen based on vertical motion anomaly over the snow cover area (figure not show). The model is integrated for 40 days in those experiments. We show the difference of winds averaged over the model days 31–40 between Experiments 1 and 2 (Figure 12). From Figure 12, it is clear that a wave pattern is induced over the midlatitude Asia, with cyclones over the region northwest of the Plateau and over North China and anticyclone in between. This pattern is similar to that observed corresponding to the western Plateau snow cover anomalies (Figures 7a and 12). The result confirms the impact of the western Plateau snow cover anomalies on the East Asian circulation through a wave pattern response over the midlatitude Asia.

5. The Source of Summer Tibetan Plateau Snow Cover Anomalies

Previous section shows an impact of summer western Tibetan Plateau snow cover anomalies over atmospheric circulation and rainfall. One question is the origin of these snow cover anomalies. In addition to snow cover anomalies in relation to snowfall in summer, the snow cover anomalies in previous months may be a source of summer snow cover anomalies due to persistence. In this section, we present the relationship between summer and preceding snow cover variations and investigate the source of the May snow cover anomalies.

The snow anomalies over the Tibetan Plateau show some persistence (Liu, Wu, Zhang, & Nan, 2014; Wu & Kirtman, 2007). This indicates that the summer Plateau snow cover anomalies may origin from preceding months. Indeed, Liu, Wu, Zhang, and Nan (2014) showed that the Tibetan Plateau snow anomalies in summer have a significant correlation with that in the preceding May. We have analyzed the grid-point correlation of snow cover between summer and the preceding April and May over the Tibetan Plateau. Significant correlation appears between May and summer snow cover over the western Plateau (figures not show). Figure 13 displays May snow anomalies obtained by regression on the west region summer snow cover index. The May snow cover displays a positive correlation over the western and southern parts (Figure 13a). The May snow water equivalent has a positive correlation in the southwestern part (Figure 13b). The results signify a contribution of May snow change to the summer snow cover anomalies. The difference in the location between snow cover and snow water equivalent may be explained by the dependence of snow cover anomalies in the mean snow mass. Large snow cover anomalies tend to occur in the border of large snow mass region (Wu & Chen, 2016). The April snow anomalies corresponding to more summer snow cover are small (figure not shown). On the other hand, the May precipitation shows positive anomalies over the western Tibetan Plateau (Figure 13c). As the mean air temperature is below 7°C in May over the western Plateau, some of the precipitation falls in the

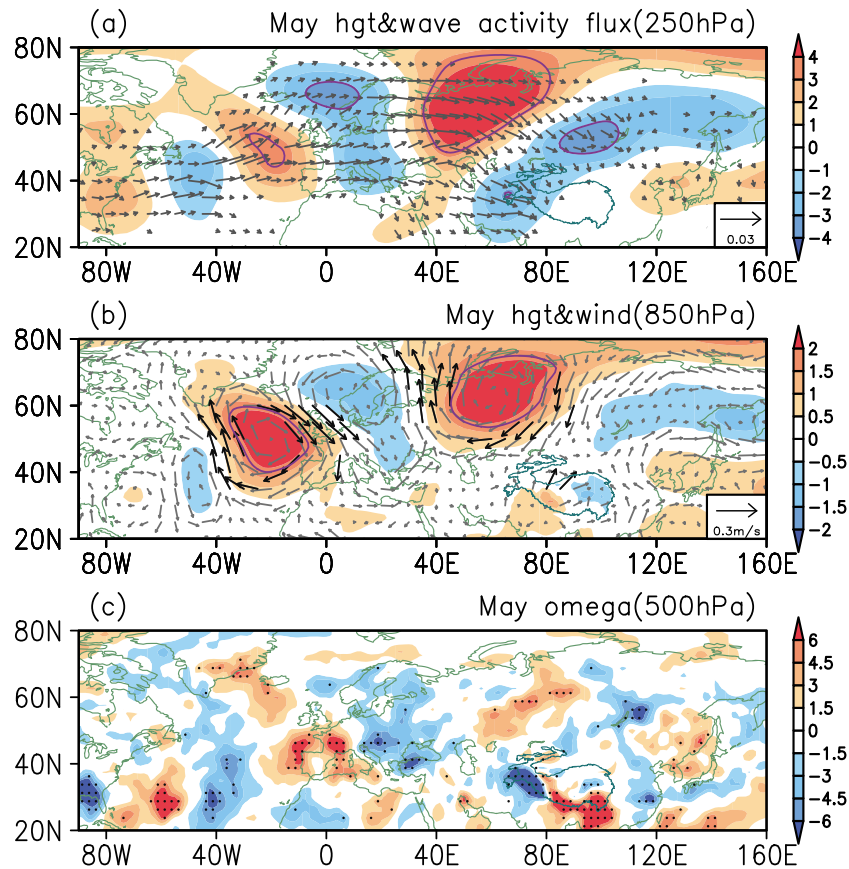


Figure 14. Anomalies of May (a) geopotential height (gpm) and corresponding wave activity flux at 250 hPa (m^2/s^2), (b) geopotential height (gpm) and winds at 850 hPa (m/s), and (c) vertical velocity at 500 hPa (Pa/h) obtained by linear regression against June-July-August interannual snow cover index in the west region. The purple contours in (a and b) and the black vectors in (b) denote geopotential height and wind anomalies significant at the 90% confidence level, and the dotted regions in (c) denote vertical velocity anomalies significant at the 95% confidence level.

form of snow (McCabe & Wolock, 2010). This indicates that the source of May snow anomalies in the west region may result from atmospheric change.

To verify the above point, we examine atmospheric circulation anomalies and wave activity fluxes (Plumb, 1985; Takaya & Nakamura, 2001) in May. Corresponding to more snow cover over the western Plateau, there is an anomalous cyclone/low pressure over the western Plateau (Figures 14a and 14b), accompanied by anomalous ascent (Figure 14c), which is consistent with above-normal precipitation/snowfall. Over the midlatitudes, a remarkable wave pattern extends from the North Atlantic to East Asia (Figures 14a and 14b). Alternative anomalous ascent and descent are present along the wave pattern with anomalous cyclone and anticyclone corresponding to the upward and downward motion, respectively.

We examine the SST anomalies in the North Atlantic Ocean to understand whether the wave pattern is related to oceanic forcing. Corresponding to more snow cover over the western Tibetan Plateau, there are positive SST anomalies off the southeast coast of North America and in the midlatitude North Atlantic Ocean and negative SST anomalies along the west coast of northern Europe and in the western part of midlatitude North Atlantic Ocean (Figure 15a). The positive and negative SST anomalies correspond to anomalous upward and downward motion in atmosphere, respectively (Figure 14c). Anomalous heating and cooling in the atmospheric column match with anomalous upward and downward motion, respectively (Figures 15b and 14c). This suggests that the SST anomalies in the North Atlantic are a forcing of the atmospheric wave pattern.

We perform numerical experiments with the barotropic model to confirm the origin of the wave pattern. Two experiments have been conducted with specified divergence and convergence anomalies. In the first experiment, climatological May mean divergence is specified to drive the model. In the second experiment,

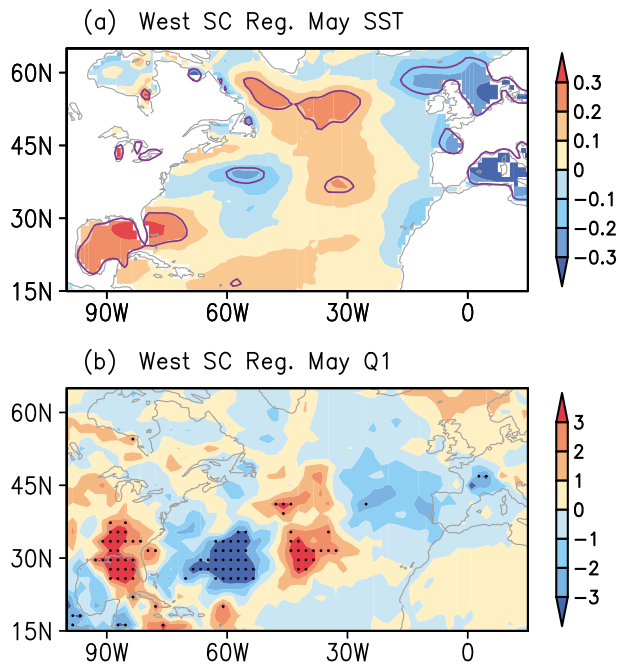


Figure 15. Anomalies of May (a) sea surface temperature (0.1 °C) and (b) Q1 (w/m^2) obtained by linear regression against June–July–August interannual snow cover index in the west region. The purple contours in (a) denote anomalies significant at the 90% confidence level, and the dotted regions in (b) denote anomalies significant at the 95% confidence level.

climatological May mean divergence plus negative convergence anomaly with a maximum intensity of $-7 \times 10^{-6} s^{-1}$ centered at 35°N, 62°W is specified. The anomaly convergence region is chosen based on the SST and vertical motion anomaly over the North Atlantic (Figures 14c and 15a). The model is integrated for 40 days. Here we show the differences of height perturbation between the two experiments averaged over the model days 35–40 (Figure 16). The model response features an obvious wave pattern along the mid-latitudes with alternative negative and positive height anomalies over the western North Atlantic through East Asia. The simulated wave pattern is quite similar to the observations (Figures 16 and 14a). This confirms a role of the North Atlantic May SST anomalies in the May snow changes over the western Tibetan Plateau through exciting a midlatitude wave pattern.

6. Summary and Discussions

The impacts of boreal winter–spring eastern Tibetan Plateau snow anomalies on the East Asian summer climate have been analyzed in many previous studies. The influence of boreal summer Tibetan Plateau snow anomalies has only been addressed in a few recent studies. The present analysis shows that boreal summer snow cover tends to have different year-to-year variations in the western and southern Tibetan Plateau. Thus, the present study investigates the roles of boreal summer snow cover anomalies in the western and southern Plateau separately and the sources of the western Plateau snow cover variations.

The local relationship between snow cover and surface heat flux variations indicates a clear signal of snow impacts on the overlying atmosphere over the western and southern Plateau in boreal summer. More snow cover leads to an increase in reflected shortwave radiation due to the albedo effect and a decrease in surface sensible and latent heat fluxes due to the interception of heat exchange. The snow impacts are verified by the atmospheric column heating changes. Obvious atmospheric cooling is identified corresponding to more snow cover.

The atmospheric circulation changes associated with the western and southern Tibetan Plateau snow cover anomalies display different features. The western Plateau snow cover anomalies are accompanied by an obvious wave pattern over the midlatitude Asia, whereas the southern Plateau snow cover anomalies are followed prominent circulation changes over the tropical Indo-Pacific regions. Over East Asia and western North Pacific, the wind and rainfall anomalies tend to display a similar distribution corresponding to the western and southern Plateau snow cover variations. These results indicate that the western and southern Plateau snow cover anomalies influence the summer rainfall variability in East Asia through distinctly different

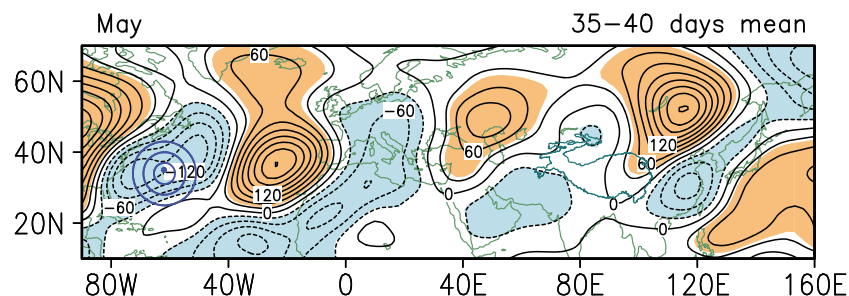


Figure 16. Barotropic model height perturbation difference (contour interval: 30 m, shaded area for difference over 40 m or below -30 m) averaged over days 35–40 and imposed idealized convergence anomaly (blue contours) for climatological mean winds in May.

atmospheric circulation changes. Further analysis illustrates that the wind and rainfall anomalies over East Asia tend to be more pronounced when the western and southern Plateau snow cover anomalies coexist with a coherent effect.

The Tibetan Plateau snow cover anomalies are accompanied by notable SST anomalies in the eastern equatorial Pacific. This suggests an effect of the SST anomalies on the East Asian wind and rainfall anomalies corresponding to snow cover anomalies. A partial regression analysis shows that the Plateau snow cover anomalies have impacts on the East Asian climate in boreal summer independent of the Pacific SST anomalies. This is confirmed by experiments of a barotropic model with specified divergence and convergence anomalies over the western Plateau.

The formation of boreal summer snow cover anomalies over the Plateau appears to be related to the persistence of snow anomalies in May. Analysis shows that the snow anomalies in May are associated with an obvious atmospheric wave pattern extending from the western North Atlantic through western Eurasia to East Asia. The North Atlantic SST anomalies may play a role in the development of this wave pattern based on observational evidence. The excitation of the wave pattern is confirmed by experiments of a barotropic model with anomalous divergence and convergence specified over the western North Atlantic.

The magnitude of area-mean snow cover anomalies in the western and southern Plateau shows different variations (Figure 2). This suggests that the western and southern Plateau snow anomalies may play alternative roles in the East Asian summer rainfall variations during different periods. Thus, a topic worthy of investigation is the interdecadal change in the impacts of the western and southern Plateau snow anomalies. A relevant issue is why the snow cover anomalies are larger in the western Plateau during some periods, but in the southern Plateau during other periods. This calls for further investigation.

In addition to the albedo effect, the snow change may affect the land hydrological process through snowmelt-induced soil moisture anomalies. To address the potential impacts of soil moisture, we obtain snow-related soil moisture anomalies by regressing JJA soil moisture at 0–10 cm against the western Plateau JJA snow cover anomalies. An obvious increase in the soil moisture is seen over the western Plateau. The JJA Q1 anomalies obtained by regression against the JJA western Plateau soil moisture anomalies are negative over western Plateau with the magnitude smaller than those with respect to western Plateau snow cover anomalies. This suggests an effect of soil moisture changes on atmospheric heating in summer. Further analysis is needed to address the above issue.

Acknowledgments

This study is supported by the National Key Research and Development Program of China grant (2016YFA0600603), the National Natural Science Foundation of China grants (41530425, 41775080, 41661144016, 41475081, and 41275081). The snow cover and snow water equivalent data were obtained from <http://nsidc.org/data/>. The NCEP/DOE reanalysis 2 data were obtained via <https://www.esrl.noaa.gov/psd/>. The JRA-55 reanalysis data were obtained from <http://jra.kishou.go.jp/JRA-55/>. The GPCP precipitation data were obtained from <https://www.esrl.noaa.gov/psd/>. The CRU temperature and cloud data were obtained from <http://www.cru.uea.ac.uk/data/>. The COBE-SST data were obtained via <https://www.esrl.noaa.gov/psd/>.

References

- Adler, R. F., Huffman, G. J., Chang, A., Ferraro, R., Xie, P. P., Janowiak, J., et al. (2003). The version-2 Global Precipitation Climatology Project (GPCP) monthly precipitation analysis (1979–present). *Journal of Hydrometeorology*, 4(6), 1147–1167. [https://doi.org/10.1175/1525-7541\(2003\)004%3C1147:TVGPCP%3E2.0.CO;2](https://doi.org/10.1175/1525-7541(2003)004%3C1147:TVGPCP%3E2.0.CO;2)
- Armstrong, R., Brodzik, M. J., Knowles, K., & Savoie, M. (2005). *Global monthly EASE-grid snow water equivalent climatology, Version 1*. Colorado USA. NASA National Snow and Ice Data Center Distributed Active Archive Center: Boulder. <https://doi.org/10.5067/KJVERY3MIBPS>
- Barnett, T. P., Dümenil, L., Schlese, U., Roeckner, E., & Latif, M. (1989). The effect of Eurasian snow cover on regional and global climate variations. *Journal of the Atmospheric Sciences*, 46(5), 661–686. [https://doi.org/10.1175/1520-0469\(1989\)046%3C0661:TEOESC%3E2.0.CO;2](https://doi.org/10.1175/1520-0469(1989)046%3C0661:TEOESC%3E2.0.CO;2)
- Brodzik, M., & Armstrong, R. (2013). Northern hemisphere EASE-grid 2.0 weekly snow cover and sea ice extent. Version 4. National Snow and Ice Data Center, Boulder, CO, digital media. Retrieved from https://nsidc.org/data/docs/daac/nsidc0046_nh_ease_snow_seaice.gd.html
- Chen, L., & Wu, R. (2000). Interannual and decadal variations of snow cover over Qinghai-Xizang Plateau and their relationships to summer monsoon rainfall in China. *Advances in Atmospheric Sciences*, 17(1), 18–30. <https://doi.org/10.1007/s00376-000-0040-7>
- Cohen, J., & Rind, D. (1991). The effect of snow cover on the climate. *Journal of Climate*, 4(7), 689–706. [https://doi.org/10.1175/1520-0442\(1991\)004%3C0689:TEOSCO%3E2.0.CO;2](https://doi.org/10.1175/1520-0442(1991)004%3C0689:TEOSCO%3E2.0.CO;2)
- Dey, B., & Kumar, O. S. R. U. (1983). Himalayan winter snow cover area and summer monsoon rainfall over India. *Journal of Geophysical Research*, 88(C9), 5471–5474. <https://doi.org/10.1029/JC088iC09p05471>
- Ding, Y., Sun, Y., Wang, Z., Zhu, Y., & Song, Y. (2009). Inter-decadal variation of the summer precipitation in China and its association with decreasing Asian summer monsoon. Part II: Possible causes. *International Journal of Climatology*, 29(13), 1926–1944. <https://doi.org/10.1002/joc.1759>
- Fasullo, J. (2004). A stratified diagnosis of the Indian monsoon—Eurasian snow cover relationship. *Journal of Climate*, 17(5), 1110–1122. [https://doi.org/10.1175/1520-0442\(2004\)017%3C1110:ASDOTI%3E2.0.CO;2](https://doi.org/10.1175/1520-0442(2004)017%3C1110:ASDOTI%3E2.0.CO;2)
- Hahn, D. G., & Shukla, J. (1976). An apparent relationship between Eurasian snow cover and Indian monsoon rainfall. *Journal of the Atmospheric Sciences*, 33(12), 2461–2462. [https://doi.org/10.1175/1520-0469\(1976\)033%3C2461:AARBES%3E2.0.CO;2](https://doi.org/10.1175/1520-0469(1976)033%3C2461:AARBES%3E2.0.CO;2)
- Harris, I. P. D. J., Jones, P. D., Osborn, T. J., & Lister, D. H. (2014). Updated high-resolution grids of monthly climatic observations—the CRU TS3.10 dataset. *International Journal of Climatology*, 34(3), 623–642. <https://doi.org/10.1002/joc.3711>
- Ishii, M., Shouji, A., Sugimoto, S., & Matsumoto, T. (2005). Objective analyses of sea-surface temperature and marine meteorological variables for the 20th century using ICOADS and the Kobe collection. *International Journal of Climatology*, 25(7), 865–879. <https://doi.org/10.1002/joc.1169>

- Kanamitsu, M., Ebisuzaki, W., Woollen, J., Yang, S. K., Hnilo, J. J., Fiorino, M., & Potter, G. L. (2002). NCEP–DOE AMIP-II Reanalysis (R-2). *Bulletin of the American Meteorological Society*, 83(11), 1631–1644. <https://doi.org/10.1175/BAMS-83-11-1631>
- Kobayashi, S., Ota, Y., Harada, Y., Ebata, A., Moriya, M., Onoda, H., et al. (2015). The JRA-55 reanalysis: General specifications and basic characteristics. *Journal of the Meteorological Society of Japan. Ser. II*, 93(1), 5–48. <https://doi.org/10.2151/jmsj.2015-001>
- Kripalani, R. H., Kulkarni, A., & Sabade, S. S. (2003). Western Himalayan snow cover and Indian monsoon rainfall: A re-examination with INSAT and NCEP/NCAR data. *Theoretical and Applied Climatology*, 74(1-2), 1–18. <https://doi.org/10.1007/s00704-002-0699-z>
- Liu, G., Wu, R., Zhang, Y., & Nan, S. (2014). The summer snow cover anomaly over the Tibetan Plateau and its association with simultaneous precipitation over the Mei-Yu-Baiu region. *Advances in Atmospheric Sciences*, 31(4), 755–764. <https://doi.org/10.1007/s00376-013-3183-z>
- Liu, G., Wu, R. G., & Zhang, Y. Z. (2014). Persistence of snow cover anomalies over the Tibetan Plateau and the implications for forecasting summer precipitation over the Meiyu-Baiu Region. *Atmospheric and Oceanic Science Letters*, 7(2), 115–119.
- Lu, R., Oh, J., & Kim, B. (2002). A teleconnection pattern in upper-level meridional wind over the North African and Eurasian continent in summer. *Tellus A*, 54(1), 44–55. <https://doi.org/10.1034/j.1600-0870.2002.00248.x>
- McCabe, G. J., & Wolock, D. M. (2010). Long-term variability in Northern Hemisphere snow cover and associations with warmer winters. *Climatic Change*, 99(1-2), 141–153. <https://doi.org/10.1007/s10584-009-9675-2>
- Ose, T. (1996). The comparison of the simulated response to the regional snow mass anomalies over Tibet, Eastern Europe, and Siberia. *Journal of the Meteorological Society of Japan. Ser. II*, 74(6), 845–866. https://doi.org/10.2151/jmsj1965.74.6_845
- Plumb, R. A. (1985). On the three-dimensional propagation of stationary waves. *Journal of the Atmospheric Sciences*, 42(3), 217–229. [https://doi.org/10.1175/1520-0469\(1985\)042%3C0217:OTDPO%3E2.0.CO;2](https://doi.org/10.1175/1520-0469(1985)042%3C0217:OTDPO%3E2.0.CO;2)
- Pu, Z., Xu, L., & Salomonson, V. V. (2007). MODIS/Terra observed seasonal variations of snow cover over the Tibetan Plateau. *Geophysical Research Letters*, 34, L06706. <https://doi.org/10.1029/2007GL029262>
- Sardeshmukh, P. D., & Hoskins, B. J. (1988). The generation of global rotational flow by steady idealized tropical divergence. *Journal of the Atmospheric Sciences*, 45(7), 1228–1251. [https://doi.org/10.1175/1520-0469\(1988\)045%3C1228:TGOGRF%3E2.0.CO;2](https://doi.org/10.1175/1520-0469(1988)045%3C1228:TGOGRF%3E2.0.CO;2)
- Si, D., & Ding, Y. (2013). Decadal change in the correlation pattern between the Tibetan Plateau winter snow and the East Asian summer precipitation during 1979–2011. *Journal of Climate*, 26(19), 7622–7634. <https://doi.org/10.1175/JCLI-D-12-00587.1>
- Takaya, K., & Nakamura, H. (2001). A formulation of a phase-independent wave-activity flux for stationary and migratory quasigeostrophic eddies on a zonally varying basic flow. *Journal of the Atmospheric Sciences*, 58(6), 608–627. [https://doi.org/10.1175/1520-0469\(2001\)058%3C0608:AFOAPI%3E2.0.CO;2](https://doi.org/10.1175/1520-0469(2001)058%3C0608:AFOAPI%3E2.0.CO;2)
- Wang, C., Yang, K., Li, Y., Wu, D., & Bo, Y. (2017). Impacts of spatiotemporal anomalies of Tibetan Plateau snow cover on summer precipitation in eastern China. *Journal of Climate*, 30(3), 885–903. <https://doi.org/10.1175/JCLI-D-16-0041.1>
- Wang, Z., Wu, R., & Huang, G. (2017). Low-frequency snow changes over the Tibetan Plateau. *International Journal of Climatology*, 38(2), 949–963. <https://doi.org/10.1002/joc.5221>
- Wu, R. (2002). A mid-latitude Asian circulation anomaly pattern in boreal summer and its connection with the Indian and East Asian summer monsoons. *International Journal of Climatology*, 22(15), 1879–1895. <https://doi.org/10.1002/joc.845>
- Wu, R., & Chen, S. (2016). Regional change in snow water equivalent–surface air temperature relationship over Eurasia during boreal spring. *Climate Dynamics*, 47(7-8), 2425–2442. <https://doi.org/10.1007/s00382-015-2972-8>
- Wu, R., & Kirtman, B. P. (2007). Observed relationship of spring and summer East Asian rainfall with winter and spring Eurasian snow. *Journal of Climate*, 20(7), 1285–1304. <https://doi.org/10.1175/JCLI4068.1>
- Wu, R., Wen, Z., Yang, S., & Li, Y. (2010). An interdecadal change in southern China summer rainfall around 1992/93. *Journal of Climate*, 23(9), 2389–2403. <https://doi.org/10.1175/2009JCLI3336.1>
- Wu, Z., Li, J., Jiang, Z., & Ma, T. (2012). Modulation of the Tibetan Plateau snow cover on the ENSO teleconnections: From the East Asian summer monsoon perspective. *Journal of Climate*, 25(7), 2481–2489. <https://doi.org/10.1175/JCLI-D-11-00135.1>
- Wu, R., Zhao, P., & Liu, G. (2014). Change in the contribution of spring snow cover and remote oceans to summer air temperature anomaly over Northeast China around 1990. *Journal of Geophysical Research: Atmospheres*, 119, 663–676. <https://doi.org/10.1002/2013JD020900>
- Wu, Z., Zhang, P., Chen, H., & Li, Y. (2016). Can the Tibetan Plateau snow cover influence the interannual variations of Eurasian heat wave frequency? *Climate Dynamics*, 46(11-12), 3405–3417. <https://doi.org/10.1007/s00382-015-2775-y>
- Xiao, Z., & Duan, A. (2016). Impacts of Tibetan Plateau snow cover on the interannual variability of the East Asian summer monsoon. *Journal of Climate*, 29(23), 8495–8514. <https://doi.org/10.1175/JCLI-D-16-0029.1>
- Yanai, M., Li, C., & Song, Z. (1992). Seasonal heating of the Tibetan Plateau and its effects on the evolution of the Asian summer monsoon. *Journal of the Meteorological Society of Japan. Ser. II*, 70(1B), 319–351. https://doi.org/10.2151/jmsj1965.70.1B_319
- Yasunari, T., Kitoh, A., & Tokioka, T. (1991). Local and remote responses to excessive snow mass over Eurasia appearing in the northern spring and summer climate. *Journal of the Meteorological Society of Japan. Ser. II*, 69(4), 473–487. https://doi.org/10.2151/jmsj1965.69.4_473
- You, Q., Kang, S., Pepin, N., & Yan, Y. (2008). Relationship between trends in temperature extremes and elevation in the eastern and central Tibetan plateau, 1961–2005. *Geophysical Research Letters*, 35, L04704. <https://doi.org/10.1029/2007GL032669>
- Zhang, Y., Li, T., & Wang, B. (2004). Decadal change of the spring snow depth over the Tibetan Plateau: The associated circulation and influence on the East Asian summer monsoon. *Journal of Climate*, 17(14), 2780–2793. [https://doi.org/10.1175/1520-0442\(2004\)017%3C2780:DCOTSS%3E2.0.CO;2](https://doi.org/10.1175/1520-0442(2004)017%3C2780:DCOTSS%3E2.0.CO;2)
- Zhao, P., & Chen, L. (2001). Climatic features of atmospheric heat source/sink over the Qinghai-Xizang Plateau in 35 years and its relation to rainfall in China. *Science in China Series D: Earth Sciences*, 44(9), 858–864. <https://doi.org/10.1007/BF02907098>
- Zhao, P., Zhou, Z., & Liu, J. (2007). Variability of Tibetan spring snow and its associations with the hemispheric extratropical circulation and East Asian summer monsoon rainfall: An observational investigation. *Journal of Climate*, 20(15), 3942–3955. <https://doi.org/10.1175/JCLI4205.1>
- Zhu, Y., Liu, H., Ding, Y., Zhang, F., & Li, W. (2015). Interdecadal variation of spring snow depth over the Tibetan Plateau and its influence on summer rainfall over East China in the recent 30 years. *International Journal of Climatology*, 35(12), 3654–3660. <https://doi.org/10.1002/joc.4239>
- Zuo, Z., Zhang, R., Wu, B., & Rong, X. (2012). Decadal variability in springtime snow over Eurasia: Relation with circulation and possible influence on springtime rainfall over China. *International Journal of Climatology*, 32(9), 1336–1345. <https://doi.org/10.1002/joc.2355>